American Mineralogist, Volume 90, pages 1801–1815, 2005

Fragmentation phenomena in populations of magmatic crystals

ILYA N. BINDEMAN*

Department of Geological Sciences, 1272 University of Oregon, Eugene, Oregon 97403, U.S.A.

ABSTRACT

Fragmentation of crystals is an important mechanism, and a component of particle dynamics in igneous and metamorphic rocks that has received surprisingly little attention. Recent advances in textural analysis, extraction techniques, digital imaging, and computer-assisted measurements enable rapid accumulation of 3D data on particle shapes and size distributions. This paper reviews fragment size distributions (FSD) that result from fragmentation: lognormal, fractal, loggamma, and Weibull; discusses their genesis mechanisms; and presents relevant examples of fragmentation from experimental physics. Next, the paper considers FSDs of feldspars on digitized images of thin sections and on published images, and quartz extracted from vesicular pumice by acid from eight well-known large-volume eruptive units. The acid solution of pumice enables examination of volume abundance, 3D shapes, proportions of fragmented crystals, and measurements of their CSDs and FSDs. FSDs were also measured in samples of welded tuff and a granite disaggregated by electric pulse. Products of syneruptive shock wave fragmentation, and fragmentation by an electric pulse are found to be fractal with large breakage probabilities, branching ratios, and fractal dimensions of 2 to 3. In contrast, most quartz fragments in pumice obey a lognormal distribution and fragmentation is driven by a melt inclusion decrepitation mechanism, which results in low breakage probability and small number (2–3) of fragments per breakage cycle. These results are consistent with one atmosphere heating experiments of quartz phenocrysts that led to melt inclusion decrepitation and caused quartz to break up into several smaller pieces collectively having lognormal FSD. Measured melt inclusion size distributions suggest decrepitation of outermost melt inclusions, and low survival rate for large inclusions, and inclusions with large radius/crystal size ratio. The modeling of periodic fragmentation of crystals with melt inclusions due to overheating and/or decompression, which may occur many times during the lifetime of a long-lived magma body, may explain concave-down, lognormal CSDs abundant in igneous rocks. The genesis of lognormality can be explained by the fragmentation algorithm of Kolmogorov (1941). Other algorithms may generate lognormal-like loggamma distributions. Fragmentation serves as an important size limiting factor, a nucleation aid, and it facilitates isotopic and trace elemental exchange.

INTRODUCTION

Fragmentation processes occur on various geologic scales from colliding planetisimals to sand grains (cf. Kapteyn and van Uven 1903; Sammis et al. 1986; Englman 1991; Nelson and Rubin 2002). Although crystal fragmentation is comparable in importance to crystal growth and nucleation, fragmentation of crystals, as one of the leading factors in transforming crystalline matter, has received surprisingly little attention in igneous and metamorphic petrology. Fortunately, particle dynamics, and particle-balance equations have received sufficient treatment in chemical engineering, where experimental, analytical, and Monte-Carlo simulations are well developed (e.g., McCoy 2001; Madras and McCoy 2002; Diemer and Olson 2002; Marchisio et al. 2003; Ferkinghoff-Borg et al. 2003). These involve nucleation, growth, breakage and aggregation in a steady state or in dynamic conditions (aerosol or soot, emulsion breakage-aggregation, polymerization-depolymerization; e.g., Spicer and Pratsinis 1996).

Many industrial processes are analogous to those in magma chambers. The coagulation processes may be similar to synneusis (e.g., feldspars: Vance 1969; olivines: Schwindinger 1999); particle coalescence during metamorphic recrystallization (e.g., zircon and monazite: Ayers et al. 2003), and formation/disaggregation of crystal clots into smaller clots or single subhedral crystals is important in some igneous systems (e.g., Best and Christiansen 1997; Jerram et al. 2003).

This paper has a goal of adding fragmentation as an important player to the overall particle dynamics of magma chambers. Best and Christiansen (1997) reviewed phenocryst breakage in more than one hundred samples of Tertiary ash-flow tuffs of the western US. They presented abundant textural evidence that clot disaggregation, syneruptive shattering, and melt inclusion explosion are the main factors for fragmentation, whereas mutual impact fragmentation of crystals is not.

The important textural tool that is available to petrologists is particle size distribution. Measured crystal size distributions, or CSDs, are commonly used in petrogenetic interpretations in

* E-mail: bindeman@uoregon.edu

0003-004X/05/1112–1801$05.00/DOI: 10.2138/am.2005.1645

nature and in crystallization experiments (e.g., Marsh 1998), but no fragment size distribution, or FSDs, have been discussed. This paper deals with particle size distribution and emphasizes the importance of breakage due to melt inclusion decrepitation in magma chambers. The study pursues several goals: (1) to describe relevant statistical distributions — lognormal, Weibull, loggamma, and fractal (power-law) — that most commonly result from geological fragmentation; (2) to review recent treatments of fragmentation processes in experimental physics that are relevant for petrology; (3) to consider FSDs measured in pumice and pyroclastic rocks; (4) to compare the natural FSD with experimental and numerical FSDs due to melt inclusion decrepitation; and (5) to argue that melt inclusion decrepitation is the leading cause of fragmentation in magma bodies that yields frequently observed lognormal FSDs and CSDs.

Particle size distributions

Fragmentation processes result in several types of size (mass)–frequency distributions, the most relevant are lognormal, fractal, loggamma, and Weibull distributions (see Appendix 1). These distributions are compared on Figure 1. Tests of statistical validity of fit ("goodness of fit") are abundant in the literature, and the reader is referred to monographs by Crow and Shimizu (1988), Aitchison and Brown (1957), and spreadsheets of Eberl et al. (2001) and K.Wohletz (http://internet.cybermesa.com/~wohletz/KWare/KWare.htm).

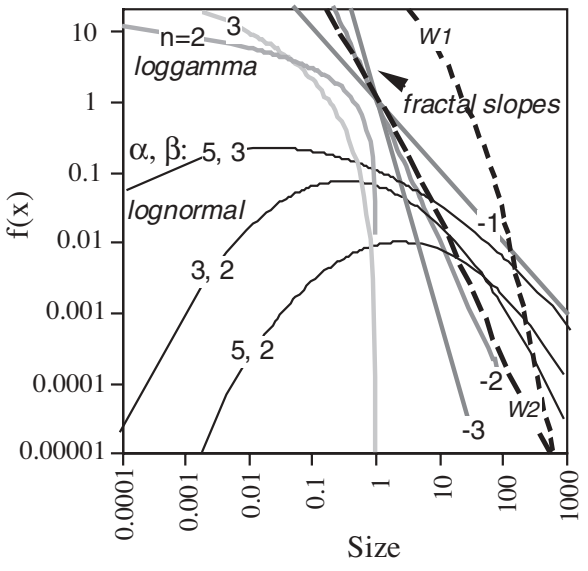

FIGURE 1. Comparison of size distributions on log-log frequency $f(x)$-generic size diagram. Note that the fractal distribution (thick gray) are straight lines, lognormal distributions (thin black) are symmetrical concave downward, and Weibull (dashed, marked W1,W2) and loggamma distributions are intermediate of the two. The small-particle end for a lognormal distribution goes through a maximum and then to 0, while a fractal distribution asymptotically approaches the ordinate; the logarithm of the value decays quicker than a power function with increasing x. Parameters used to construct each distribution (see Appendix for equations) are: for lognormal — the mean (α) and standard deviation (β); for fractal are fractal slopes — C = 1 in all cases; for Weibull distribution — number of particles (N_T = 325), shape parameters — γ = –0.5 (W1) and γ = –0.86 (W2); for loggamma distribution (here defined on $0 < x < 1$) — α(the mean) = 1, n = 2, and 3.

Distribution genesis laws

Lognormal distributions, which were popular for the first half of the last century (Ahrens 1954) can be generated by the law of proportional effects (Kapteyn and van Uven 1903), which states that the variation of a parameter X (e.g., linear size or volume of a crystal) is proportional to its previous state:

$$\frac{X_{j+1} - X_j}{X_j} = \varepsilon \quad (1)$$

where ε is a small and random parameter (e.g., increment of growth). Equation 1 defines intrinsic *size-dependency*, i.e. larger crystals grow faster, yielding lognormal (concave-up, positively skewed) size-frequency distributions (see Aitchison and Brown, 1957, p. 22–23). Size-dependent (vs. constant-rate) growth of crystals was recently advocated by Eberl et al. (1998) and Kile and Eberl (2003, and references therein) as explaining many naturally occurring CSDs.

For the fragmentation process, the law of proportionate effects may be written as:

$$\frac{X_{j+1} - X_j}{X_j} = -\varepsilon \quad (2)$$

which is analogous to the mechanism of Kolmogorov (1941), in which fragmentation involves splitting a particle in two random pieces, then saving one and performing breakage on the other. The process approaches theoretical lognormal as the number of steps increases. Other fragmentation and selection algorithms that affect multiple particles at each step (Epstein 1947; Atchison and Brown 1957) also yield lognormal distributions. Dacey and Krumbein (1979) and Middleton (1970) presented a series of other algorithms of breakage and selection and, in particular, considered an important case in which breakage affects particles that formed in different generations. They demonstrated that the final distribution is actually factorial (*loggamma)* that approaches lognormal for large number of breakage steps. Many natural fragmentation data follow lognormal statistics, including distribution of boulder sizes, grains in sandstones (Middleton 1970; Mahmood 1973) and soils (Barak et al. 1996); cataclastic quartz grains in some fault gouges (Engelder 1974; Sammis et al. 1986; An and Sammis 1994), and in ores (Kolmogorov 1941).

The *fractal*, or *power-law*, distribution is primarily generated by a process that is scale-invariant. Thus, the products of this process are also scale-invariant and result from fractal (branching-tree) crack propagation upon brittle deformation. The intensity of branching ultimately defines the fractal dimension D (see Appendix 1), and is dependent on a number of physical and material parameters discussed below. Fragmentation was shown to obey fractal statistics for many materials and fragmentation algorithms (Turcotte 2002). Scale-invariant texture is commonly observed in sandstone clasts from fault gouges. Sammis et al. (1986) explained this observation by the comminution mechanism, which involves spallation: upon contact of two grains of equal size, one grain breaks into n (>8) pieces and the process repeats itself on smaller scales yielding a fractal dimension (D) of 2.5. Many phenomena in geology and geophysics are scale-

invariant: drainage networks, fault and earthquake distribution, ore deposits, asteroid sizes, crater diameters on planets, etc. [see Englman (1991) and Turcotte (1997, 2002) for further discussion].

A *Weibull distribution* is also generated by a series of branching (scale-invariant) cracks, but the breakage probability is a function of fragment size. Therefore, the Weibull distribution has properties of both fractal and lognormal distributions, and was originally derived empirically by Rosin and Rammler (1933) who considered size fragment distribution of coal upon breakage and noted that smaller particles were better "protected." Brown and Wohletz (1995) advocated a Weibull distribution for processes resulting in an excess of fine particles, and for phreatomagmatic explosions in particular (Wohletz et al. 1989). Mathematically and graphically the Weibull distribution looks intermediate between lognormal and fractal (see Fig. 1 and Appendix), but it does not have advantage of being dimension- or scale invariant.

Fragmentation in experiments

The physics and technology literature provides important analogue for geological fragmentation. Experimental fragmentation has been shown to cause lognormal, fractal, or Weibull size distributions. Ishii and Matsushita (1992) dropped long thin (750×2 mm) glass rods from different heights and measured lengths and masses of all fragments after a single episode of brittle fragmentation. This experiment was designed to test a simple (e.g., Kolmogorov's) case of one-dimensional breakage, where mass distribution is identical to length. At small falling heights, the fragments obeyed a lognormal distribution, whereas at higher falling heights (i.e., at stronger fragmentation intensity), the fragments followed fractal distribution.

Meibom and Balslev (1996) fragmented 2-dimensional clay discs, and discovered similar relationships. Sotolongo-Costa et al. (1996) studied fragmentation of mercury spheres dropped from different heights, and found that lognormal distribution is characteristic for low falling heights, and fractal for larger heights. A change in fragmentation mechanism with increasing height (intensity of shock) was proposed.

Fragmentation mechanisms and the resulting size distributions may not depend on only the shock intensity or the material crushed (e.g., gypsum, soap, paraffin, or potato, Oddershede et al. 1993), but also on shape (Meibom and Balslev 1996). Notice that the issue of dimensionality and the definition of "size" are also important in fragmentation. Sotolongo-Costa et al. (2000) and Ishii and Matsushita (1992) described smaller and larger fragments by two fractal relationships with different values of the fractal D constants, explained by the dimensional crossover.

Unlike single-episode breakage described above, time-series comminution serves as an additional dimension in fragmentation. Tavassoli and Shirvani (2000) presented several numerical binary fragmentation models with the probability of further breakage proportional to the size of a fragment, and were able to generate both scale-invariant (fractal) and lognormal size distributions that are stable on long time-scales.

Thus, the physics literature suggests that both lognormal and fractal particle size distributions can be produced in experiments, and it seems that more energetic and multi-stage process favors a fractal distribution, which has a multitude of small particles. The theoretical explanation for this comes from the maximum-entropy principle (for review of this topic, see Englman 1991).

Natural examples of phenocryst breakage

Below, this paper addresses crystal- and fragment size distributions measured in igneous rocks. "Fragment" is defined as any part of a single crystal, and its classification as "broken" is established by visual inspection in 3D. This work does not consider disaggregation of crystal clusters and glomeroporphyritic aggregates abundant in many igneous rocks (Best and Christiansen 1997; Jerram et al. 2000, 2003) as aggregation-disaggregation mechanisms involve different physical processes from breakage of the lattice of a single crystal. Table 1 summarizes fragmentation mechanisms that are relevant for igneous processes, their timing, algorithm, intensity, and the resulting statistical distributions, which are discussed in the text.

Table 1. Relevant igneous fragmentation mechanisms and resulting fragment size distributions (FSD) discussed in text

Process	Timing	Relevant references	FSD this work	Breakage algorithms	Branching ratio
Melt Inclusion decrepitation					2–5
A. overheating	preeruptive	0, 2	lognormal	multi-stage, dissolution of smaller fragments	
B. decompression	preeruptive	0,1,3,9	lognormal	multi-stage?	
	syneruptive		loggamma	single stage	
Shock wave fragmentation	syneruptive	0,1,6,7	fractal Weibull	single stage multi-stage?	10–1000
Mutual impact fragmentation	syneruptive	1	fractal	single stage	10–1000
Dissagregation of glomeroporphyric clots	preeruptive syneruptive posteruptive (flow shear)	1,4	preexisting CSD	multi-stage	~2–10?
Flow shear	syneruptive posteruptive	5	?	multi stage	<2–3?
Electric pulse	?	0, 8	fractal	single stage	>>1000

Notes: 0 = this work; 1 = Best and Christiansen (1997); 2 = Zhang (1998); 3 = Tait (1992); 4 = Jerram et al. (2003); 5= Allen and McPhie (2003); 6 = Pallister et al. (1996); 7 = Wohletz et al. (1989); 8 = Rudashevsky et al. (1995); 9 = Lipman et al. (1997).
Syneruptive refers to the time in the exit channel, posteruptive refers to time after exit, preeruptive refers to magma chamber; branching ratio is the number of fragments per breakage cycle (typical ranges).

Methods of phenocryst and fragment extraction and 3D measurements

Two-dimensional imaging in thin sections, photo images, and rock slabs are traditionally employed for crystal size distribution studies, including feldspars imaged for this work. Various methods of stereological corrections to 3D (e.g., Higgins 1994) are employed. Both 2D and stereologically corrected 3D (as spheres, using the program StripStar) data of feldspars are presented in this work, because feldspars are impossible to extract from glass by acid solution, and plagiodgse vs. sanidine are best identified from each other in thin sections.

Several techniques have recently been employed to measure quantitatively crystal shapes, size distributions, relative positions, and orientations of crystals and their fragments in 3D. These methods include: optical imaging of orientation and size of microlites in obsidian under the microscope (Castro et al. 2003); light crushing, sieving, winnowing; careful, layer-by-layer sample dissection (Jerram et al. 2003; Gualda et al. 2004); and X-ray tomography (Ketcham and Carlson 2001). These techniques are variably labor-intensive and/or expensive but do provide important information on relative position and clustering of crystals and fragments. This work is based on a more-expeditious (but hazardous!) method of acid extraction as is described in the Appendix of Bindeman (2003) and briefly below.

Acid solution. The glassy and vesiculated nature of pumice enables rapid extraction of insoluble or weakly soluble phenocrysts and their fragments by acid (HF and HBF_4) digestion. The advantage of this method is quantitative extraction of acid-resistant crystals of quartz, zircon, magnetite, and olivine, which allows determination of volume and particle concentrations per gram of magma, examination of shapes, sizes of crystals, and reconstruction of their 3D size distribution. Acid solution does not dissolve small crystals, and possibly is the most retentive method for quantitative extraction of the smallest (~10 μm) acid resistant crystals of quartz and zircon (see Line and Aradine 1937; Bindeman 2003; Gualda et al. 2004). To examine relative positions of crystals and fragments prior to dissolution, thin sections for denser-welded pumice clasts were studied, and physical dissection of more vesicular pumice clasts by layer-to-layer removal of vesiculated glass around phenocrysts and fragments was performed. Few crystal aggregates were found in pumice and scoria samples examined in this work, and importantly, most crystal fragments were surrounded by volcanic glass suggesting that fragmentation occurred above the glass transition. Similar results were obtained recently by Gualda et al. (2004) in Bishop pumice clasts that were studied by X-ray tomography.

Electric pulse disaggregation. Another novel method for extracting crystals quantitatively, which is tested here, is electric pulse disaggregation (Rudashevsky et al. 1995). This technique utilizes difference in piezoelectric properties of minerals and aggregates under the influence of high-voltage electric discharge, which disaggregates a rock along preexisting grain boundaries and cracks. Electric pulse disaggregation is ideal for quantitative extraction of small highly conductive ore minerals of complex shapes (e.g., platinum, gold), small non-conductive accessory minerals (zircon, monazite), and fossils, while preserving their shapes (Saini-Eidukat and Weiblen 1996; Cavosie et al. 2004) for subsequent textural analysis. Because of this potential, the electric pulse technique was tested here for its value in CSD and FSD studies of major minerals. Two samples, denser welded Lava Creek Tuff (Yellowstone), and Cathedral Peak granodiorite (Yosemite), were subjected to 100 kV electric pulse disaggregation in water by placing a sample between the cathode and anode of an XRD source at the University of Minnesota, in the laboratory of Prof. Paul Weiblen. FSDs were measured in disaggregated samples by sieving and weighing, and are apparently fractal (Fig. 2). Similar distributions may characterize samples shocked by lightning, i.e. in fractured rocks around desert fulgurites. However, the electric pulse technique failed to separate phenocrysts from glass in welded tuff, or quartz from feldspar in granite, and thus seems not to be a promising quantitative method to separate major phases, and it is not used further in this study.

Imaging and FSD measurements. A Scion-NIH Image program and a digital camera attached to a microscope were used to make a series of images of thousands of acid-extracted phenocrysts and fragments, and to measure their lengths, widths, areas, and perimeters. The resolution of optical imaging was chosen to be in 200–500 pixels/mm and varied from sample to sample, or thin section to thin section, depending on the smallest crystal observed to ensure that there is no loss of smallest crystals due to resolution.

Collected data were exported to a spreadsheet for further

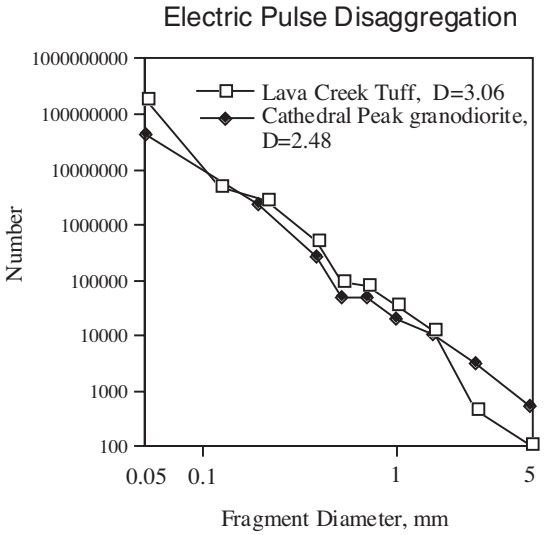

FIGURE 2. Fragment size distribution of two samples disaggregated using an electric pulse. The sample of Lava Creek Tuff (Yellowstone) consisted of volcanic glass (80%), feldspars (10%), quartz (7%), and other minerals (3%); Cathedral Peak granodiorite (Yosemite National Park) is made of feldspar (70%), Fe-Mg minerals (20%), and quartz (7%). Each sample initially weighted 333 g and fragmented into ~10^8 fragments spanning >2 orders of magnitude in size in the course of ~15 min of electric pulsing. Fragments were sieved into 10 size fractions, and average mesh diameter of each fraction is plotted on the X-axis. Notice that fractal distribution of fragments is apparent in these log-log coordinates with slopes (fractal dimension *D*) of 2.48 and 3.06, typical and higher than that for fragmented granites (Turcotte 1997). These distributions imply that preexisting cracks in both the tuff and granodiorite were fractal in nature, as electric disintegration follows preexisting grain boundaries and cracks (Rudashevsky et al. 1995).

calculations, and results were plotted. The lognormality and acceptance criteria were demonstrated by applying χ^2 (*Chi*-square) and Kolmogorov-Smirnov (KS) tests, using the "Galoper" set of Excel spreadsheets (Eberl et al. 2001). Fractal distribution is evidenced by plotting the distribution on a log-log diagram and fitting a straight line; the slope defines the fractal dimensions. Lognormal, loggamma, and Weibull distributions in these coordinates are concave downward (Fig. 1). Acid solution enables confident quantitative extraction of small quartz crystals and fragments down to 10 µm, which is important for making judgements about curvature on the FSD diagrams.

Because feldspars react with acid, FSD of feldspars were studied in thin sections in 2D. Measurements of fragment dimensions were performed manually (>1000 measurements total) in order to distinguish plagioclase from sanidine and quartz.

Observation of broken phenocrysts in pumice

Fragmentation processes differ in what FSD they generate, and the important goal of the present paper is to develop observational tools to distinguish between syneruptive fragmentation by shock waves, and fragmentation due to melt inclusion decrepitation.

Proportion of breakage. Studied samples (Table 2) range in the proportions of broken vs. unbroken crystals. Pumice clasts from different ash-flow tuffs and even different cooling units of the same tuff (e.g., Bishop tuff) contain strikingly different proportion of broken vs. unbroken crystals. On one extreme, about one half of quartz from late-erupted Bishop tuff pumice studied here is broken. Quartz crystals in rhyolites from Katmai, regardless of being pyroclastic (Layer A) or extrusive (Novarupta), are almost entirely unfragmented. Typically, late-erupted, deeper, and thus more greatly decompressed clasts of the same eruption contain a larger proportion of broken crystals. Pumice clasts in ignimbrites typically contain more broken crystals than the coeval and rapidly quenched ash-fall pumice clasts, or lavas and domes. Overall, the proportion of broken phenocrysts in studied vesicular pumice clasts is lower than what is described for ignimbrites and tuffs elsewhere (Best and Christiansen 1997; Pallister et al. 1996, see below). These observations suggest that the breakage process is unit-specific, clast-specific, and mineral specific. Unlike CSDs of unbroken crystals presented in Bindeman (2003), FSDs do not characterize and fingerprint the eruptive unit as a whole.

Quartz. Table 2 presents visually estimated percentages of broken crystals of quartz, which were acid-extracted from pumice clasts, taken from several well-known and voluminous ash-flow sheets. Quartz fragment shapes range from near-euhedral, half-crystals to elongated and boomerang-type splinters surrounded by concoidal fractures, or narrow two-dimensional wedges. Fragment size distributions were measured in two clasts (Fig. 3) where whole crystal size distributions were previously measured to be lognormal (Bindeman 2003). The reduction in maximum and mean sizes is apparent on Figure 3, but there is a lesser abundance of the smallest fragments. This is interpreted to mean that each breakage episode of millimeters-size crystals generated several fragments of tenths of millimeter size, but

TABLE 2. Characterization of sizes, abundance, particle concentration, and proportion of broken crystals of quartz that was acid-extracted from major ash-flow tuffs and lavas

Tuff sample	unit	Eruptive *T* (Qz-Mt) *T* °C	Zrc sat *T* °C	Crystal content vol%	SiO_2 wt%	Qz vol%	n Qz cm^{-3}	Mean Qz mm	Broken crystals %	Experimentally cracked at 800 °C		Sample appearance	Pumice diameter cm
Lower Bandelier (LBT), Toledo Caldera, NM, 600 km^3, 1.61 Ma													
LBT-10	Late	771		25	75	8.7	77	1.16	20	2 from 8	25%	VPC, white	6
LBT-4	Early	737		10	77	4.4	1129	0.33	5	6 from 12	50%	VPC, white	6
Bishop (BT), Long Valley Caldera, CA, 750 km^3, 0.76 Ma													
LV-27	Early	714	735	9	78	3.8	66	0.83				WT, gray	
BC97-16	Early	754	735	9	78	2.1	73	0.74	60	4 from 4	100%	VPC, white	10
LV-751	Late	762	761	15	76	6.4	98	1.08	50	1 from 6	16%	VPC, white	10
LV-748	Late	817	776	13	73	5.8	85	1.16	20	6 from 11	55%	VPC, pink	10
LV-3	Late	763	767	27	73	11.8	132	1.11	80	1 from 7	14%	VPC, pink	25
LV-13	lava		801	15	72	1.6	42	0.72	20	0 from 5	0%	VL, pink	
Lava Creek (LCT), Yellowstone Caldera, WY, 1000 km^3, 0.64 Ma													
LCT-3a, A	Early	800	809	11	78	7.8	780	0.47	7	0 from 8	0%	WPC, pink	30
LCT-4, B	Late	912	863	22	74	16.4	162	1.10	45	0 from 8	0%	WPC, pink	30
YL-4	lava		882	9	76	2.0	61	0.34	10	0 from 6	0%	OL, black	
Huckleberry Ridge(HRT), Big Bend Caldera, WY, 2500 km^3, 2.04 Ma													
HRT-3a, A	Early		863	19	77	9.8	113	1.05	50	0 from 7	0%	WPC, pink	>30
HRT-1, B	Late		868	26	74	12.1	179	0.95	65			WPC, pink	n.d.
HRT-C, C	Late		897	21	75	8.2	185	0.87	50			WT, gray	
Mesa Falls (MFT), Island Park Caldera, ID, 300 km^3, 1.3 Ma													
MFT-1			800	37	78	18.5	88	1.39	35	7 from 9	78%	WPC, pink	
Ammonia Tanks (AT), Timber Mountain Caldera, NV, 1000 km^3, 11.45 Ma													
TM-15	Early	762	809	14	76	7.0	83	0.95	30	5 from 8	63%	VPC, white	n.d.
TM-17	Late	870	842	20	73	2.9	171	0.62	50	1 from 7	14%	VPC, pink	n.d.
TM-24	lava	754	776	7	76	2.3	241	0.49	15	0 from 6	0%	VL, white	
Katmai-Valley of 10,000 Smokes rhyolite, AK, 8-12 km^3,1912 AD													
KTM-3	Early		790	2	77.4	0.9	83	0.53	17	0 from 9	0%	VPC, white	30
Novarupta	Late	949	786	2	76.6	0.5	87	0.59	5	0 from 6	0%	VL, gray	
Yongest Toba Tuff, Toba Caldera, Indonesia, 2800 km^3, 0.074 Ma													
YTT-102	Early	752	762	27	75.6	8.8	43	1.15	65	0 from 4	0	VPC, white	15

Notes: Oxygen isotope T (°C) estimates are based on quartz-magnetite oxygen isotope thermometry for the same clasts (see Bindeman and Valley, 2001, 2002); T (Zrc sat) is zircon saturation temperature. N is measured particulate abundance per 1cc of melt. Sample appearance related to its post-eruptive cooling, welding, and oxidation duration is as follow: VPC = is vesiculated pumice clast; WPC is welded pumice clast, WT = is welded tuff, OL is obsidianic lava, VL is vesiculated lava. Experimentally cracked refers to the reheating and decrepitation experiments of this study (Figs. 6 and A2, Appendix 2).
See Bindeman (2003) for additional information for these samples.

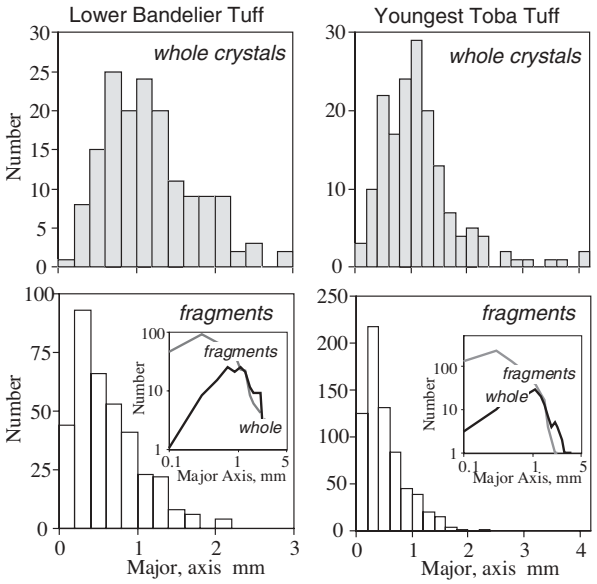

FIGURE 3. Fragment size distribution of quartz from Lower Bandelier Tuff (sample LBT10) and the Youngest Toba Tuff as compared to the unfragmented whole-crystal CSD in the same clasts (see Table 2). Both whole crystals and fragments can be fitted by lognormal distributions with high confidence level (>10%, KS test) for both long and short axes. Insets show the same data plotted in log-log coordinates to illustrate lognormality. Fragmentation is interpreted to result from melt inclusion decrepitation (see text).

apparently only a few fragments of a hundredth of a millimeter. The fragment size distributions are also statistically lognormal with a high confidence level of >10% using the KS test.

Zircon. Zircon crystals acid-extracted from the same clasts (Table 2, also see Fig. 1 of Bindeman 2003) do not show significant breakage, though singly terminated crystals were observed in some cases. Importantly, strongly elongated (L/W >5) zircons are absent (but are observed elsewhere), and may indicate one-dimensional breakage followed by broken edge annealing, as is seen in the pictures of Poldervaart (1956).

Feldspars. Broken feldspars are abundant in volcanic rocks as is easily seen in their truncated zoning patterns in thin sections (Best and Christiansen 1997; Allen and McPhie 2003), and feldspar is possibly the most frequently fragmented phenocryst owing to its cleavage. Feldspars dissolve in HF and HBF_4 acids; X-Ray tomography poorly distinguishes plagioclase from sanidine, and feldspars from quartz, and has poor resolution at small sizes (e.g., Gualda et al. 2004). Thus, feldspar fragments were examined here in 2D in thin sections and images (Fig. 4).

Best and Christiansen (1997) described examples of broken phenocrysts of feldspars in many tuff units of the western US. They presented outlines of fragmented and unfragmented sanidine phenocrysts on their Figure 1 and plagioclase on Figure 2, which they called phenoclasts. These two figures were digitized and analyzed in Scion-NIH Image program. On fragment frequency-distribution plots, phenoclasts are skewed toward smaller sizes, larger length to width ratio (L/W), and smaller area/perimeter ratio (Figs. 4A and 4B). The latter parameter can be used for statistical recognition: feldspar fragments are commonly narrow, with small areas and large irregular perimeters, but in other cases, good cleavage of feldspar prevents clear-cut distinction of some more regular fragments from elongated microlites, especially when done in 2D in thin sections. On a length-frequency diagram, sanidine and plagioclase fragments define concave-downward lognormal distributions with high confidence level (Fig. 4C). Best and Christiansen (1997) also experimentally broke phenocrysts by firing them from a shotgun. The odd splinter-like shape of fragments in these experiments (their Figs. 10–11) made them to conclude that mutual impact fragmentation upon collision of crystals during violent eruption is not a dominant process in nature.

The world's largest ash-flow sheet, the crystal-rich Fish Canyon tuff of Colorado (5000 km^3, 28.5 Ma) contains a feldspar crystal population that is almost entirely broken (Lipman et al. 1997; Bachmann et al. 2002). Figure 4D plots fragment size distributions manually measured in thin sections of two samples: a welded outflow sheet sample of Fish Canyon tuff, and its precursor tuff - Pagosa Peak dacite that was erupted less violently, possibly by low-column fire-fountaining (Bachmann et al. 2000). Measurement of plagioclase FSD in thin sections followed by stereological correction to 3D. Regardless of the mode of eruption, both samples exhibit similar, statistically lognormal FSDs.

Other minerals and fragmentation susceptibility. Qualitative observations on other minerals, including olivine, pyroxenes, amphiboles, and micas, performed in Fish Canyon tuff, Laki eruption of Iceland, basalts and scoria of Kamchatka, and elsewhere suggest less dramatic fragmentation and/or rapid and effective crystallographic overgrowth following fragmentation. A ranking of minerals by their tendency to fragment by melt inclusion decrepitation (see below) can be constructed based on observations in thin sections, pumice and scoria:

Feldspars ≥ Quartz > Olivine >Mica> Amphiboles = Pyroxenes > Zircon ≥ Mt

Similar observations on fragmentation susceptibility in lavas and domes as seen in 2D in thin sections were recently made by Allen and McPhie (2003). The ability of a mineral to break is seen to depend on the mineral bulk and shear modulus (e.g., zircon vs. mica); its ability to capture and retain melt inclusions (MI) (quartz vs. zircon); cleavage (quartz vs. feldspar); and shape (flaky mica vs. pyroxene). However, syneruptive fragmentation by shock waves leads to a different fragmentation susceptibility sequence, as the smallest shards of amphibole are abundant in Pinatubo pumice (Pallister et al. 1996).

Syneruptive shockwave breakage of Pinatubo phenocrysts

Pallister et al. (1996) and other researchers who studied dacitic products of the pyroclastic eruption of Pinatubo in the Philippines (1991, 8–11 km^3) noted that pumice lapilli fall into two distinct petrographic groups. (1) Dominant (80–90% of total volume) white, crystal-rich (35–50%) lapilli consisting of moderately broken 1–2 mm phenocrysts of plagioclase, hornblende, quartz, Fe-Ti oxides, accessories, and anhydrite, which are in compositional and textural equilibrium with the host glass. And (2) less abundant, gray, phenocryst-poorer (~20%) pumice with

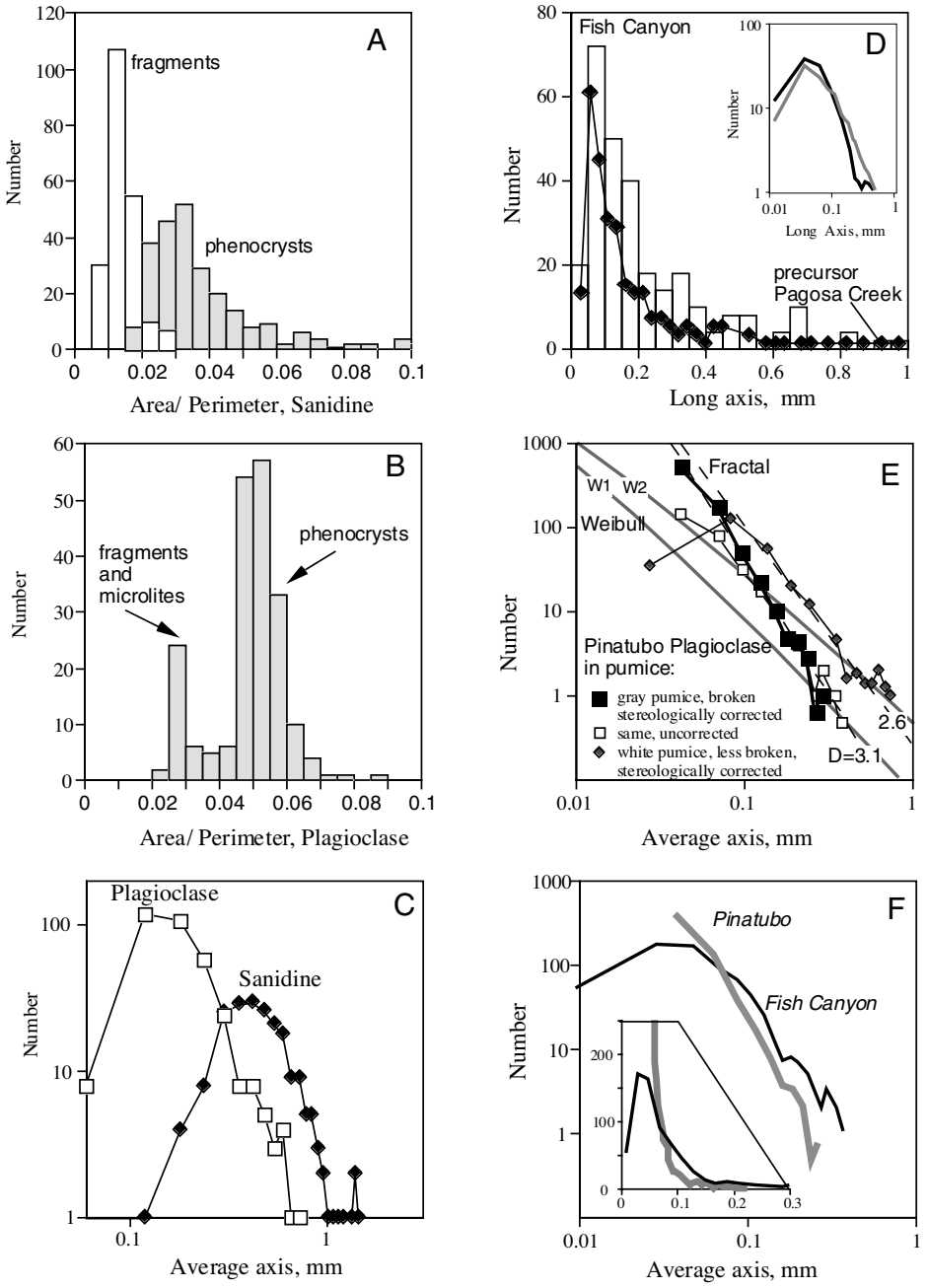

FIGURE 4. Fragmentation characteristics of feldspars in pyroclastic rocks. **A-C:** Fragmented sanidine and plagioclase phenocrysts (phenoclasts) from Figures 1 and 2 of Best and Christiansen (1997); phenoclasts were identified based on their irregular shapes. **D-F**: Measured (by the author) fragment size distribution of plagioclase in Fish Canyon tuff and in Pinatubo pumice. (**A**, **B**) Area/Perimeter for phenocrysts vs. phenoclasts demonstrating significantly smaller area/perimeter ratio for phenoclasts. (**C**) size-frequency diagram defining lognormal distributions for both feldspars with >10% confidence level, KS test. (**D**) Fragment size distribution in Fish Canyon tuff (sample FCT-54, bulk tuff), as compared to the smaller volume precaldera precursor tuff of the same composition (Pagosa Peak dacite, sample BFC-34; see Bachmann et al. 2002 for sample description); these two samples have similar FSD and are statistically lognormal (>10%, KS test), see inset. (**E**) Plagioclase FSD data for broken phenocrysts in Pinatubo gray and white pumice (Pallister et al. 1996); Weibull distribution curves are also shown for comparison (γ parameters are –0.86 and –0.92). The measured data were stereologically corrected to 3D as spheres, the procedure that does not affect lognormality, see Appendix 1. The smallest crystals in gray pumice were counted with ± 1 μm resolution in 5 fields of view of thin section volume 0.061 $mm^2 \times 0.035$ mm and then normalized to the imaged area that was used for FSD measurements of the larger size fragments in the same thin section; number uncertainty of this procedure is estimated as ±50%, but it does not change the conclusion that the smallest fragments are the most abundant by number, and the distribution is fractal. **(F)** Comparison of Fish Canyon tuff (lognormal) and Pinatubo gray pumice (fractal) FSDs on a log-log plot after stereological correction to 3D. Notice significant differences in curvatures of these distributions seen on log-log and linear plots, and compare this to Figure 1.

Fig. 5 Bindeman E-F, 2005 CORRECTED

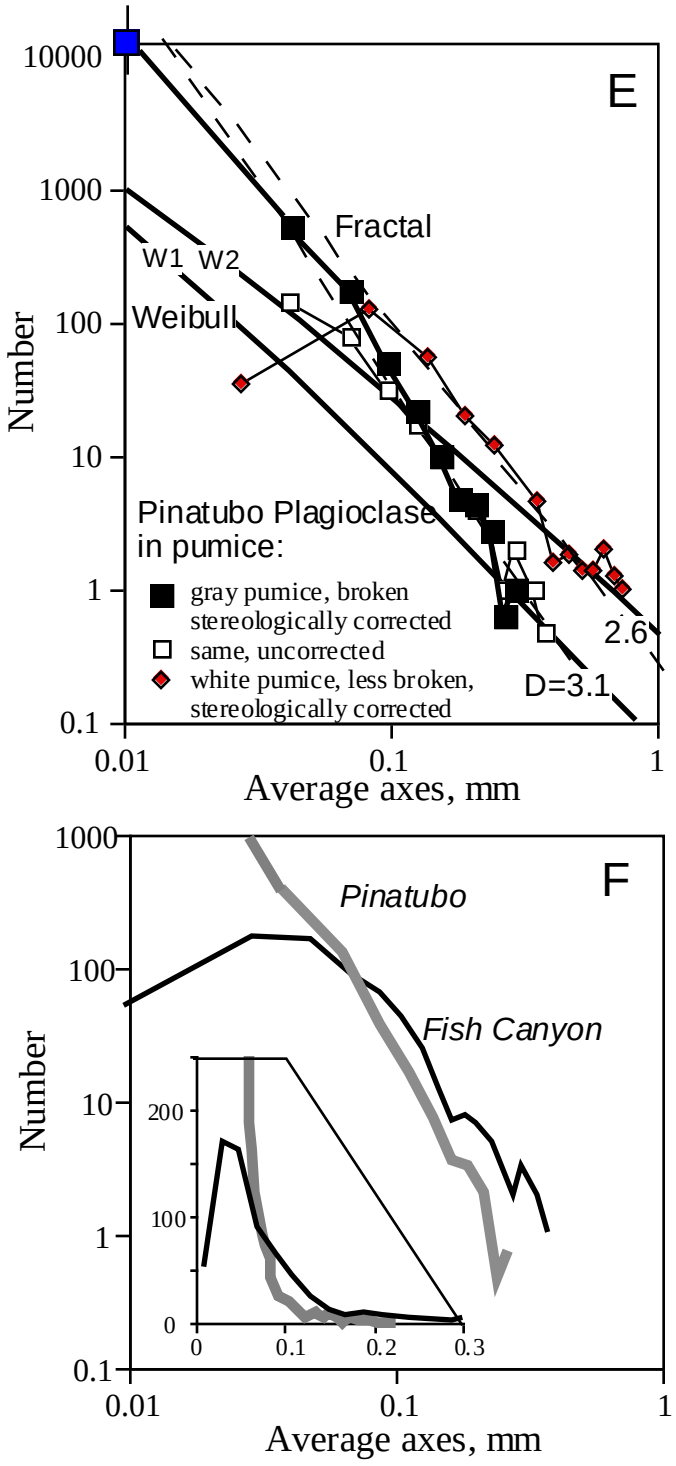

the same phenocrysts, which are severely broken and reduced in size down to several-micrometer fragments. Differences in fragmentation behavior of plagioclase, hornblende, and quartz have been documented at millimeter to micrometer scales. Crystal fragments of all minerals as small as 1–5 micrometers are recognized in the same thin sections used in that study provided by Dr. Pallister. Thin sections and BSE images (Pallister et al. 1996, Figs. 10–11; Luhr and Melson 1996, Fig. 1) demonstrate that most fragments are entirely surrounded by glass, or glass+bubble. For the highly fragmented gray pumice, the number of crystal fragments increase with decreasing size down to several micrometers in size. In white pumice, the glass is largely clear, although some small fragments are nonetheless present.

Phenocryst breakage is invoked to be the dominant process explaining texture, the character of vesicularity, crystal sizes, crystal shapes, and even chemical differences between the two dominant types of pumice. Pallister et al. (1996) suggested that breakage happened by a variety of syneruptive mechanisms (shock waves, choked flow, violent vesiculation) in the eruptive conduit, probably minutes before pumice formation and quench. Citing subtle chemical differences in pumice glass, Luhr and Melson (1996) proposed that crystal breakage started to happen a bit earlier, perhaps hours to days before, or during the violent magma mixing that triggered the 1991 eruption. Mixing and/or dissolution of smaller fragments could have contributed to slightly more mafic composition of glass in gray pumice. Luhr and Melson (1996) also noted that fragmented crystals are ubiquitous for the entire 30 ka volcanic record of Pinatubo.

Pallister et al. (1996, Figs. 10–11) presented X-Ray maps of Al for typical white and gray pumices that are appropriate for identification of plagioclase crystals down to the scale of ~10 μm. These images were used to measure FSDs of plagioclase manually (307 crystals in gray pumice and 150 in white pumice in total). Additionally, the smallest plagioclase fragments (less than 10 μm in size) were counted separately by measuring them in the same thin sections. The FSD graphs are plotted in Figure 4E, and are fitted with fractal and Weibull distributions. Fragments span >2 orders of magnitude in size, and the most abundant size class is <10 μm and which is shown by a big open square on Figure 4E. For the gray pumice, the data points can be clearly approximated by a straight line with a negative slope D = 2.85 to 2.9, and a fractal distribution thus can be inferred. For the white pumice, the smallest crystals are not overly abundant in BSE image and in glass within examined thin section, yielding a concave up lognormal distribution.

In this Pinatubo example, the syneruptive feldspar fragmentation in gray pumice yields rather high fractal dimensions, which may be explained by good cleavage of feldspars. Experimental impact breakage of other minerals and rocks yields similar fractal constants (2 to 3); for example in granites, which are mostly feldspars, D = 2.5 (Turcotte 1997). Experimental breakage of volcanic glass yields D = 1.89 (Turcotte 1997), fewer fragments, and more "cohesive" behavior. It is interesting to note that the electric pulse disaggregation yields even higher D values (3.06, Fig. 2).

When compared on the same plot (Fig. 4F), Pinatubo gray pumice feldspars and feldspars from the Fish Canyon tuff (Fig. 4D) show clear distinction in their FSD: not only does the Pinatubo data conform with a straight-line fractal distribution, it also increases with decreasing size far steeper than the Fish Canyon data (see Fig. 4F); however, the Fish Canyon feldspar FSD follows concave-down lognormal distribution.

Experimental and numerical breakage due to melt inclusion decrepitation

Below, this work demonstrates the importance of melt inclusion (MI) decrepitation in fragmentation of crystals in magma bodies, as this process is seen to dominate fragmentation for long-lived batholith-size magma systems such as those sampled by the pumice in large-volume ash-flow sheets (Table 2). Crystals in these bodies may have persisted for tens to hundreds of thousands of years, over which time multiple episodes of thermal and pressure fluctuations could have caused crystals to fragment and, later, to recrystallize. To understand fragmentation by MI decrepitation and its effects on FSD, simple MI decrepitation experiments with quartz crystal were performed at 1 atm in an oven, and numerical models of breakage were developed.

Experimental fragmentation by MI decrepitation

The simple heating experiments are described in Appendix 2 (Electronic supplement), and results are given below. The goal of heating experiments was to determine: (1) the proportion of breakage, referred to below as the probability of breakage; (2) the number of pieces into which each crystal broke (Fig. 5), called the branching ratio; and (3) the weight and fragment size distributions. These parameters were compared with those resulting from fragmentation by syneruptive shock waves.

The initial crystal size distribution of all 130 initially unbroken crystals of quartz, which ranged in size from 0.2 to 2.75 mm, was lognormal with a high confidence level (Fig. 6A). After 1 hour at 800 °C in an oven, many crystals broke, but quartz crystals from different eruptions differ dramatically in their probability of breakage (Fig. A2, Appendix), which is seen to depend on a number of specific parameters discussed in the Appendix 2.

In all cases, broken crystals contained a melt inclusion in the center of the radial concoidal cracks that separated two parts of the same crystals before they fell apart (e.g., Fig. 5). Importantly, each crystal broke only into a small number of fragments, typically 2–3 (Fig. 6C), and most fragments were unequal in size with parents generating a dominant and a smaller offspring(s) (Figs. 6C–6D, A2

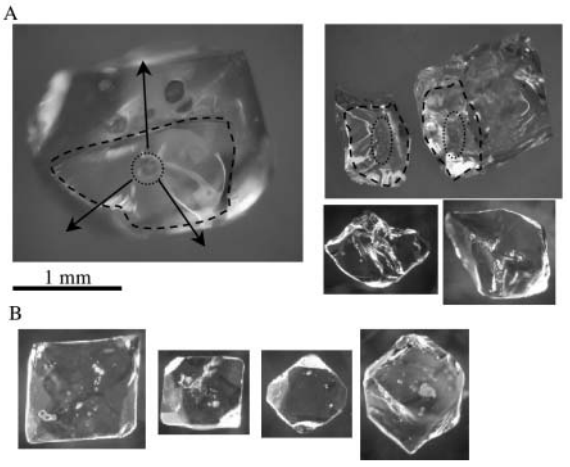

Figure 5. (**A**) Photomicrograph of fragmented quartz with radial and concoidal fractures around exploded melt inclusion, and typical small fragments. (**B**) other acid-extracted quartz crystals from the Lower Bandelier Tuff that did not fragment.

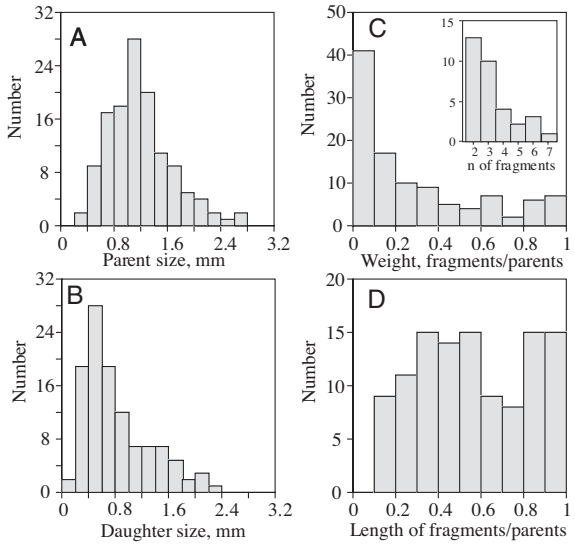

FIGURE 6. Histograms of size distributions of all quartz crystals used in decrepitation experiments (**A**), and fragment size distribution (**B**) resulting from A for crystals that broke due to melt inclusion decrepitation (Fig. A2, Appendix). Both distributions are lognormal with >10% confidence level using KS test. (C) and (D) are weight and length ratio of fragments relative to the parent. Inset in C shows the histogram of number of fragments generated per breakage. Notice that melt inclusion decrepitation results in breaking chips off quartz crystal that are 5–30% of its weight but 30–60% of its initial length (see Fig. 5). This length is larger than fragment sizes in shock-wave syneruptive or electric pulse disintegration (Figs. 2 and 4), or in fault gauges.

in Appendix 2[1]) with weights adding up to the original parent crystal. However, only few 0.05 mg and smaller fragments were generated. Examination of quartz crystals after breakage suggests decrepitation of those melt inclusions that are closest to the crystal edge; the interior inclusions are retained (Fig. 5). This probability explains why each initial crystal sheds off smaller pieces, and not fragments of equal size. This observed process is significantly different from quartz breakage during compression against other quartz grains of similar size in fault gauges, where far smaller particles in greater numbers are produced (Sammis et al. 1986; Cashman and Cashman 2000).

The observed decrepitation of outer and larger melt inclusions is in agreement with calculations of Tait (1992) and Zhang (1998). Tait (1992) examined elastic properties of common igneous phenocrysts (quartz and olivine) and demonstrated that small to medium (<50–100 μm) melt inclusions trapped within typical size of 0.5–3 mm crystals should survive a few kilobar isothermal decompression upon eruption. However, larger melt inclusions, or melt inclusions trapped near crystal edges when radius of inclusion, R_i, is close to the radius of the host R_h, will cause the crystal to fragment. Overpressure by heating is as important as decompression; quartz overheating by 40 °C is equivalent to 1 kb decompression.

Bodnar et al. (1989, their Fig. 3) performed a series of heating-stage decrepitation experiments on individual synthetic fluid inclusions in hydrothermal quartz, and quantified empirically the relationship between the inclusion size and the critical overpressure: small (<10 μm) inclusions survive up to 4 kbar overpressure while the majority of >10 μm inclusions decrepitated at <1 kbar overpressure. Wanamaker et al. (1990) similarly discussed crack formation and rehealing in olivine upon decompression. These authors have also considered the influence of formation and homogenization temperatures, inclusion shape, time of exposure, and decrepitation and healing behavior of cracks, and demonstrated significant ranges in these parameters (e.g., <50 to >100 °C for overheating) for decrepitation to occur. These observations are compatible with our simple oven heating experiments, which collectively demonstrate that the probability of breakage is phenocryst-specific, clast-specific, and unit-specific (see Appendix 2), and probabilistic treatments of fragments generated in this way is justified.

[1] Deposit item AM-05-026, Appendix 2. Deposit items are available two ways: For a paper copy contact the Business Office of the Mineralogical Society of America (see inside front cover of recent issue) for price information. For an electronic copy visit the MSA web site at http://www.minsocam.org, go to the American Mineralogist Contents, find the table of contents for the specific volume/issue wanted, and then click on the deposit link there.

Numerical fragmentation

A series of Monte-Carlo fragmentation simulations were performed on a population of 500 crystals. The algorithm (see captions to Fig. 7) was meant to simulate crystal breakage by melt inclusion decrepitation to produce a small number of relatively large fragments per breakage event, as is illustrated on Figure 7A. The FSDs of weights and average linear dimension are plotted on Figures 7B and 7C. After 3–4 breakage cycles of the same population, a positively skewed distribution developed, and it can be approximated by a lognormal fit with a high confidence level. The number of breakage cycles necessary to achieve a theoretically lognormal FSD is dependent on the initial CSD, and the fragmentation algorithm (sequence of breakage events). If the CSD is initially lognormal, as many CSDs are, the first generation FSD is lognormal as well. When the initial CSD departs maximally from lognormal, and is left-skewed for example (Fig. 7), a stable lognormal distribution developed after only 4–5 breakage cycles, thus reflecting a "memory effect" of an initial CSD. The algorithm of our numerical breakage differs from that of Kolmogorov (1941), who saved one particle at each cycle and this generated a mathematically strict lognormal distribution (see Eq. 2) after n cycles. Such a process may result when decrepitating melt inclusions produce small shards that are in turn dissolved in the magma. If this does not happen and small fragments are retained and counted, then distributions became skewed to the left too much and the goodness of lognormal fits decrease, but they remain "lognormal-like." Dacey and Krumbein (1979) demonstrated that a loggamma distribution may be more appropriate to use in these situations. On a log-log diagram (e.g., Fig. 1), the generated FSDs are concave down.

MELT INCLUSION SIZES AND HOST CRYSTAL SIZES

Despite significant effort in interpreting melt inclusions (MI) and their chemical or isotopic content, no measurements exist on melt inclusion size distributions, and their relationship to the host crystal sizes. However, in the context of the present study, MI sizes, abundances, and size distributions record "explosive potential" of a crystal or a crystal population, and MI size distribution may provide further evidence of time-integrated episodes of their capture by growth, and destruction by fragmentation.

Figure 8 presents measurements of all melt inclusions in quartz from two pumice clasts of late-erupted Bishop and Lower Bandelier tuffs, and the sizes are plotted vs. size of their host crystal. Making these measurements for a transparent mineral like quartz is relatively easy by focusing at different optical depths and taking photographs that can be digitized and analyzed easily using the program NIH-Scion Image. Other minerals may require 2D imaging and conversion, but these procedures will be less precise. The observations and discussion below are concentrated on quantifying physical parameters such as MI size, host quartz size, MI size vs. host size, and their bearing on fragmentation probability based on theoretical work on melt inclusion overpressures and cracking by Tait (1992) and Zhang (1998).

Melt inclusions in quartz span more than two orders of magnitude in size from a few micrometers to >200 μm. The number of MI increases with decreasing MI size down to the optical resolution level of <1–2 μm. However, most larger MI occurs in larger crystals, whereas small MI occur indiscriminately in large or small quartz (Fig. 8). The abundance of MI in quartz ranges from 0.05 to 1 vol%, with the majority (90%) in the range 0.05–0.5 vol%, and abundance decreases with increasing quartz size. The Radius

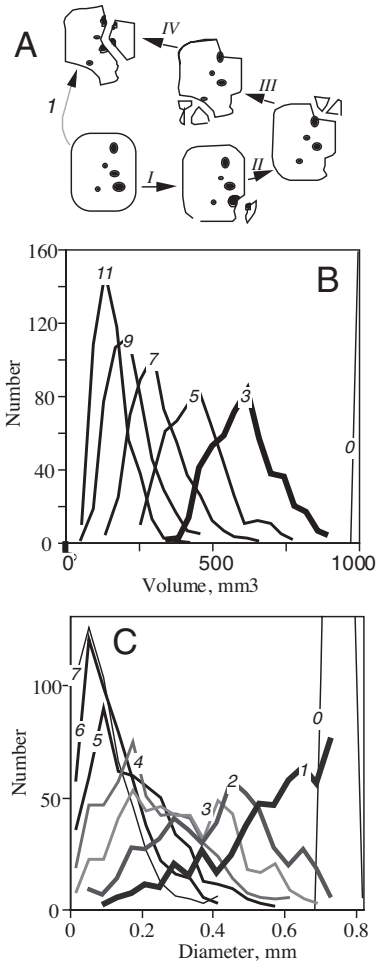

FIGURE 7. Results of Monte Carlo modeling of successive fragmentation of an initial near-normally distributed population of 500 crystals using equation 2 in the text. (**A**) conceptual model of successive melt inclusion decrepitation and chipping off smaller fragments similar to what is observed (see Fig. 6); notice that multiple fragmentation events (I-IV) are equivalent to a single more intense breakage episode marked 1. (**B**) Breakage of 1 cm^3 volume according to Kolmogorov's algorithm ($\varepsilon = 0.3 \times$ random number, see Eq. 2) when only larger remaining pieces are counted and others are discounted (e.g., dissolved). The process approaches theoretical lognormal distributions as the number of steps increases. Goodness of fit increases from <1% for cycle 1, 5% for cycle 3, to >10% for cycles 5 and higher using KS test. Lognormality applies to both volumes and lengths due to the additive property of logarithms (see Appendix 1). (**C**) Successive FSD of *all* fragments resulting from fragmentation of a near-normal population of crystals with 0.76mm mean diameter, (±0.02 1 st. dev). The breakage probability is 0.5, the number of fragments per breakage cycle is 2. Following each breakage, the population is randomized and 500 crystals participate in the next cycle of breakage, all crystals (large and small) are counted. Notice successive size reduction and transition from right to left skewness. FSDs of cycles 4–5 are statistically lognormal (>5%, KS test); but progressively depart from lognormality at higher cycles as the number of smaller fragments is becoming too excessive. However they remain "lognormal-like": concave up and skewed to the right. Dacey and Krumbein (1979) demonstrated that such distributions represent a mixture of loggamma distributions.

of inclusion/Radius of host (R_i/R_h) quartz parameter ranges from <0.02 to >0.18 (Fig. 9A), but most MI have small R_i/R_h (90% are 0.02 to 0.08).

The statistically determined concentration, distribution of sizes, and R_i/R_h of MI enable calculations of the probability of decrepitation of MI of variable R_i/R_h in quartz (Fig. 9A). Significant overpressures result from either decompression or overheating of MI (Fig. 9B), but overpressure in excess of few hundred bars is usually accommodated by a series of small cracks around the melt inclusion, with linear dimensions on the order of MI size (e.g., Wanamaker et al. 1990; Tait 1992). Inclusions with exceptionally large R_i/R_h (e.g., >0.25) can crack their host quartz easily at even the smallest perturbations; the smallest inclusions are most likely to survive. This may explain the low statistical abundance of large inclusions in smaller quartz (Fig. 8), and low occurrence of large R_i/R_h inclusions (Fig. 9A): they have decrepitated and fragmented their host quartz. The same argument may apply to large inclusions that occur near the crystal surface (within 1–2 diameters), as episodes of overpressure (heating or decompression-induced) will result in their partial or complete decrepitation with fragmentation of the host quartz, and with generation of two fragments of different size (see Fig. 7A). This is what is observed in the above decrepitation experiments. Thus, the interpretations made here based on MI sizes are complementary to the conclusions derived from consideration of fragment size distributions (Fig. 3–4), and from decrepitation experiments (Fig. 5–6). These observations call for a more dynamic view of melt inclusion capture and retention balance as a part of the overall crystal population dynamics when fragmentation is involved.

DISCUSSION

It is illustrated above that fragmentation processes affect population balance and dynamics of igneous phenocrysts; lognormal FSDs result from MI decrepitation and can be distinguished statistically from fractal FSDs, which result from syneruptive fragmentation by shock waves. Syneruptive breakage yields high branching ratios (number of fragments) and fractal dimensions, *D*, ranging from 2 to 3, which can be used as a tool to predict breakage probabilities as is illustrated and explained on Figure 10, using fractal distribution genesis law (Turcotte 2002; see Appendix 1). Melt inclusion decrepitation yields small number of fragments, and is not likely to be fractal in origin as, if such, the *D* should be very low numbers <1 (Fig. 10). This is an important distinction that results from differences in the energetics of underlying processes.

Syneruptive fragmentation has received attention and description (e.g., Wohletz et al. 1989; see Fig. 4E). I concentrate below on a more "hidden" process of periodic crystal fragmentation due to melt inclusion decrepitation that may characterize particle dynamics in many evolving, and long-lived magma bodies, and that may explain abundant lognormal and lognormal-like CSDs, which are seen in many igneous rocks.

The genesis of lognormal and loggamma distributions due to MI decrepitation

The conclusion of the present work is that crystal size evolution and particle dynamics involve fragmentation due to decrepitation of melt inclusions, which may happen due to de-

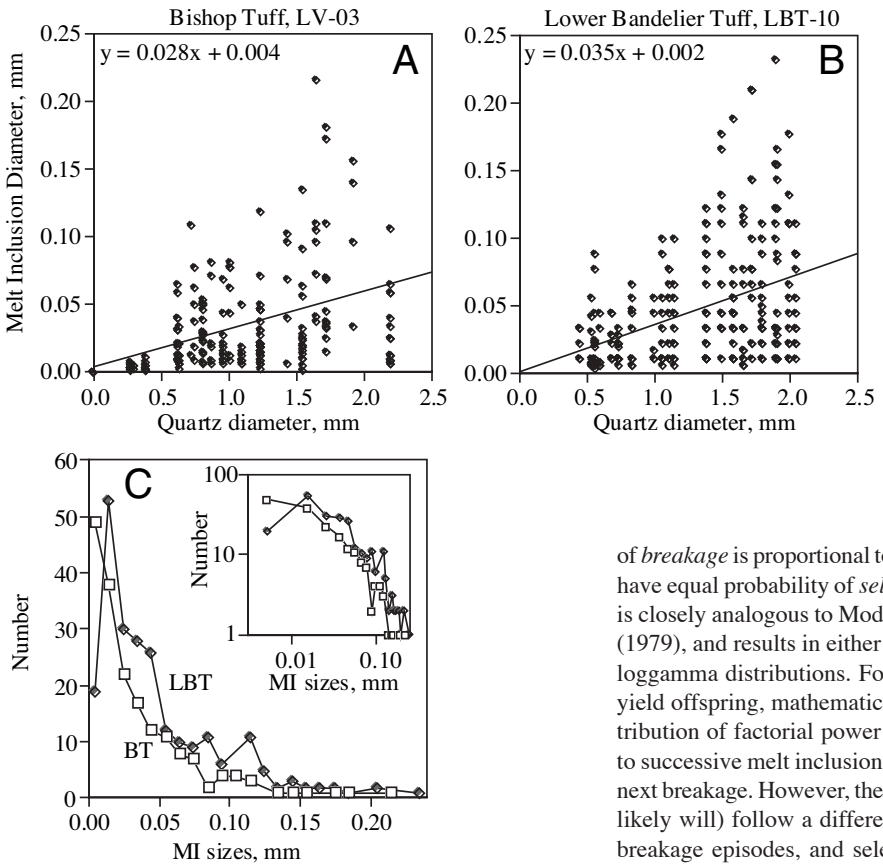

FIGURE 8. (**A, B**) Measurements of melt inclusion diameters as a function of the size of their host quartz crystal from two individual pumice clasts of the Bishop tuff (BT) and the Lower Bandelier tuff (LBT). The optical resolution is 1–2 μm and the number of <1 μm melt inclusions is uncertain. Notice that smaller melt inclusions are present regardless of quartz size, larger melt inclusions are found predominantly in larger quartz. This relationship is interpreted here to indicate fragmentation process in which large melt inclusions survived only in larger crystals. (**C**) MI size distributions, the inset plots the same data on a log-log scale illustrating concave down lognormal shape.

compression or overheating, and the resulting FSDs will follow lognormal or loggamma statistics.

Differing breakage algorithms. The genesis algorithms distribution resulting from melt inclusion decrepitation in igneous rocks is analogous to the theory of classification (Aitchison and Brown 1957), and to the origin of clastic sediments (e.g., Middleton, 1970; Mahmood, 1973). In both cases, breakage and selection for the next step of breakage are involved, and a combination of breakage algorithm *and* selection algorithm, is what determines the final mathematically significant distribution. For example, consider a succession of breakage events for a population of particles of uniform size into two particles with sizes X and 1-X, coupled with dissolution of one particle either by weathering, stream transport, or magmatic dissolution upon reheating (which caused the MI decrepitate in the first place). This algorithm generates a strictly lognormal distribution of the remaining population (Kolmogorov 1941; Aitchison and Brown 1957). If the small particles persist, as they would, for example, during isothermal decompression, the resulting distribution depends on whether the daughter particles participate in the next episode of breakage. For magmatic crystals, it is most likely that the "rejected" particles will be smaller and also melt inclusion-free and will not participate in the next episode of breakage, whereas the big crystal may experience the next episode of breakage (see Fig. 7A). The reduction in the crystal size brings other MI closer to the surface. This can be modeled if the probability of *breakage* is proportional to size of the particle, but all particles have equal probability of *selection* for breakage. This algorithm is closely analogous to Models 1 and 2 of Dacey and Krumbein (1979), and results in either lognormal or a mixture of factorial loggamma distributions. For example, each large particle may yield offspring, mathematically consistent with loggamma distribution of factorial power *n* after *n*-1 cycles of breakage due to successive melt inclusion decrepitations and selection for the next breakage. However, the neighboring particle may (and most likely will) follow a different branching algorithm, number of breakage episodes, and selection, and thus it will approach a different loggamma or lognormal function.

The loggamma distributions, shown on Figure 1 also are concave down, and its mixture with lognormal, and/or subsequent dissolution or annealing of the smallest particles by ripening will make the final mixed distribution closely analogous to lognormal. In either case of overheating or decompression, the process generates "hump-up" positively skewed distributions that are identifiable on FSD plots.

Pre-eruptive or syn-eruptive fragmentation? The abundant lognormal distributions found for quartz and feldspar fragments in this work with documented deficiency of smaller fragments (see Figs. 3 and 4) may indicate that overheating was the leading mechanism of fragmentation with subsequent dissolution. Overheating is most consistent with these processes occurring in a magma chamber, and that the lognormal FSDs were quenched within pumice by the eruption. The decompressive decrepitation-breakage episode will generate abundant smaller particles and the distribution may follow loggamma distribution with greater multitude of smaller particles over lognormal. Syneruptive shock waves will additionally increase the relative abundance of the smallest particles, further departing the final distribution from lognormal.

Other processes generating concave-down CSD. It is important to stress that the use of frequency-size distributions to infer particular genesis mechanisms is treacherous. Many processes in the magma chamber are proportionate and selective, and lead to the commonly observed concave-up, right-skewed distributions. Nucleation and growth control sizes and population

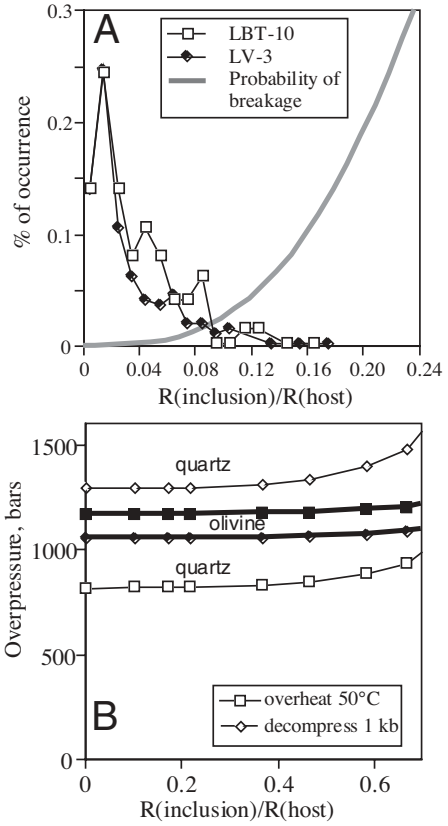

FIGURE 9. (**A**) Histograms of radius of inclusions to the radius of the host crystal for the same pumice clasts as shown on Figure 8, and the calculated probability of breakage. The latter parameter is simply the probability of random occurrence of a spherical melt inclusion of radius R_i within $2R_i$ distance from the surface of crystal with radius R_h. The overpressure in these inclusions will be sufficient to overcome the strength of the host quartz's crystal and cause breakage of smaller chunk(s) of linear dimensions that are comparable to the inclusion diameter (see Fig. 6, and A2 Appendix 2 for comparison). Notice that the calculated breakage probability increases as a power of 3, while the measured occurrence of inclusions with large R_i/R_h decreases likewise. This relationship is interpreted to indicate destruction of large R_i/R_h inclusions due to multiple episodes of overheating and/or decompression. (**B**) Calculated overpressures (P_{in}-P_{out}) as a result of isothermal decompression of quartz-rhyolitic melt and olivine-basaltic melt for 1 kb, and isobaric heating by 50 °C. Equation 21 of Zhang (1998) was programmed, and elastic and thermal expansion parameters are those used by Tait (1992). Notice that heating by a few tens of degrees produces several hundred bars overpressure; the cracking limit for quartz and olivine are on the order of several hundred bars, and magnitude depends on preexisting microcracks (Tait 1992). Overheating can be caused, for example, by magma mixing with hotter magma.

densities of crystals in a variety of crystallization environments (Randolph and Larson 1988; Marsh 1998; McCoy 2001; Eberl et al. 2001), and many of these processes, such as size-dependent growth, growth with significant growth-rate dispersion, size-dependent solution-reprecipitation, annealing of smaller crystals by Ostwald ripening or communicating neighbor mechanisms (e.g., Higgins 1998; Eberl et al. 2002), may also yield lognormal, or

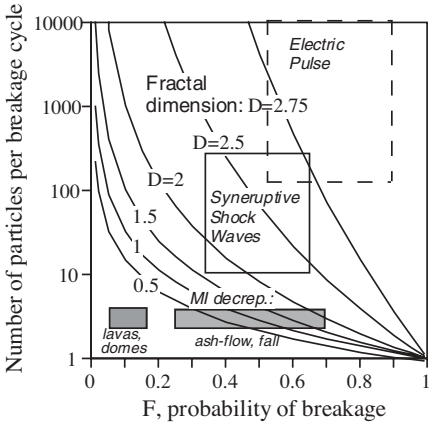

FIGURE 10. The diagram relating fractal dimension (D) with breakage probability (F) and the number of particles per breakage cycle, which serves as a measure of breakage intensity (see Turcotte 1997; Armienti and Tarquini 2002, see Appendix 1). Due to semi-log coordinates, fractal slopes are exponential. The syneruptive breakage by shock waves is fractal in nature [e.g., examples from Pinatubo (Pallister et al. 1996; Best and Christiansen 1997)] and has $D \sim 2$–2.75, which yields $N = 20$–50, and $F = 0.3$–0.6 on this diagram. Disintegration by the electric pulse is also fractal (see Fig. 2) and is estimated to have $D \sim 2.5$–3, $N >> 100$, and $F > 0.8$–0.9, but less than 1. Breakage by melt inclusion decrepitation results in a small number of fragments per cycle (2–3, see Fig. 6C inset), but variable breakage probability; for lavas and domes it is <0.15 (e.g., Allen and McPhie 2003), for ignimbrites it is typically ranging from 0.25–0.7 (e.g., Fig. 6). Such low intensity process has prohibitively small fractal dimension (0.5–1.5), and is not fractal but lognormal in nature.

concave downward lognormal-like distributions. For example, these processes, rather than fragmentation, yield lognormal CSDs of zircons extracted from pumice by acid solution, which are found to be most common in igneous rocks (Bindeman 2003). These examples suggest that alone or in combination, fragmentation and nucleation/growth/annealing mechanisms, may cause lognormal and lognormal-like distribution of crystals in igneous rocks. The lognormality alone should not be used to make genetic interpretations, but fragmentation should become a component of size distribution studies and of numerical simulations of textural origins.

Examples of fragmentation and particle dynamics in evolving magma chambers

Magma mixing and magma recharge. Magma mixing may cause heating of differentiated magma with phenocrysts by the heat of the newly intruded, less-differentiated hotter magma, the extent of which is dependent on magma proportions, crystal content, efficiency of thermal transport, and initial temperatures. Chamber recharges by hotter magmas may result in mass decrepitation of MI and crystal fragmentation in the colder magma, especially if there is an initial overheat of colder silicic magma due to delay in crystal dissolution and hence latent heat consumption (e.g. Fig. 5 in Bindeman 1993). This provides a sufficient mechanism of >50 °C overheating, and should lead to mass decrepitation of typical MI causing crystal fragmentation;

the FSD may subsequently anneal and be mistaken for "normal" volcanic CSD. Injection of silicic magmas into hotter mafic bodies is another possibility for overheating and crystal fragmentation.

Rejuvenation of magma bodies. Fish Canyon Tuff, the rejuvenated granitic batholith, consists almost entirely of broken phenocrysts (Figs. 4D and 4E), which are interpreted to result from decrepitation of MI (Lipman et al. 1997). The tuff has been generated by remobilization of the mush of crystals by the heat and volatiles of newly intruded mafic magma, as proposed by Bachmann et al. (2002) and Bachmann and Bergantz (2003). The heating by an estimated ~40 °C could have been an important factor in mass decrepitation of MI still in the magma chamber, which not only caused crystals to fragment, but also, perhaps, has led to smaller crystal dissolution and yielded lognormal FSD (Figs. 4D and 4E).

Recognition of fragments. Crystal fragments may be present as unrecognized parts in many phenocrysts. Since many fragments, especially in plutonic rocks, may get recrystallized and resorbed following fragmentation, they are often mistaken as simple resorbed cores, especially when examined in 2D sections. This is particularly true for plagioclase, a mineral with good cleavage, which exhibits reverse and complex zoning patterns and core-rim structures in magma mixing environments. Commonly observed albite-richer crystals with reverse zoning may have suffered significant reheating by tens of degrees, but such overheat should generate fragments in accordance with observations above (see Fig. 9B). If they are subsequently held in the main body of magma with minimal temperature fluctuations, recrystallization by Ostwald or Communicating Neighbors ripening mechanisms will affect only the smallest (ca. <20 μm) fragments (Cabane et al. 2001, 2005). Optical examination of crystals using a universal stage, chemical and cathodoluminescence imaging (e.g., Peppard et al. 2001), examination of zoning truncations, and wavelet-based correlation of crystal zoning (Wallace and Bergantz 2002) may serve as labor-intensive tools of choice to recognize fragments and decipher past fragmentation episodes in magmatic crystals. Fragmentation may also play an important role in the development of the time-integrated CSDs, and should be taken into account when quantifying crystal populations, and recognizing past fragmentation episodes. Finally, fragmentation of crystals by the melt inclusion decrepitation mechanism may be an important geological feedback mechanism of magmatic growth that prevents igneous crystals from growing infinitely large.

This paper introduces a new acronym—FSD—and suggests that fragmentation by melt inclusion decrepitation mechanism is an important process that yields lognormal and lognormal-like FSDs and CSDs in igneous systems, and especially in large silicic magma bodies.

ACKNOWLEDGMENTS

I thank Dennis Eberl for discussions about the importance of proportionate growth; Paul Weiblen for help with the electric pulse disaggregation; John Pallister and Olivier Bachmann for sending samples of Fish Canyon and Pinatubo pumice, respectively; Fred Anderson, John Valley, and John Eiler for collaboration and advice; and Jon Castro and Laura Baker for comments. Reviews by Dougal Jerram, Olivier Bachmann, and Eric Christiansen, as well as the exhaustive comments and editorial handling by Richard Ketcham are gratefully acknowledged.

REFERENCES CITED

Aitchison, J. and Brown, J.A.C. (1957) The lognormal distribution, 176 p. Cambridge University Press, U.K.

Ahrens, L.H. (1954) The lognormal distribution of elements (a fundamental law of geochemistry and its subsidiary). Geochimica et Cosmochimica Acta, 5, 49–74.

Allen, S.R. and McPhie, J. (2003) Phenocryst fragments in rhyolitic lavas and lava domes. Journal of Volcanology and Geothermal Research, 126, 263–283.

An, L.-J. and Sammis, C.G. (1994) Particle size distribution of cataclastic fault materials from Southern California: a 3D study. Pure and Applied Geophysics, 143, 203–227.

Anderson, A.T. (1990) Hourglass inclusions: theory and application to the Bishop Rhyolitic Tuff. American Mineralogist, 76, 530–547.

Armienti, P. and Tarquini, S. (2002) Power-law olivine CSD in lithospheric mantle xenoliths. Lithos, 65, 273–285.

Ayers, J.C., deLaCruz, K., Miller, C., and Switzer, O. (2003) Experimental study of zircon coarsening in quartzite ± H_2O at 1 GPa, 1000 °C, with implications for geochronological studies of high-grade metamorphism. American Mineralogist, 88, 365–376.

Bachmann, O. and Bergantz, G.W. (2003) Rejuvenation of the Fish Canyon magma body: A window into the evolution of large-volume silicic magma systems. Geology, 31, 789–792.

Bachmann, O., Dungan, M.A., and Lipman, P.W. (2000) Voluminous lava-like precursor to a major ash-flow tuff: low-column pyroclastic eruption of the Pagosa Peak Dacite, San Juan volcanic field, Colorado. Journal of Volcanology and Geothermal Research, 98, 153–171.

——— (2002) The Fish Canyon magma body, San Juan volcanic field, Colorado: Rejuvenation and eruption of an upper-crustal batholith. Journal of Petrology, 43, 1469–1503.

Barak, P., Seybold, C.A., and McSweeney, K. (1996) Self-similitude and fractal dimension of sand grains. Soil Science Society of America Journal, 60, 72–76.

Best, M.G. and Christiansen, E.H. (1997) Origin of broken phenocrysts in ash-flow tuffs. Geological Society of America Bulletin, 109, 63–73.

Bindeman, I.N. (1993) A practical petrological method for the determination of volume proportions of magma chamber refilling. Journal of Volcanology and Geothermal Research, 56, 133–144.

——— (2003) Crystal sizes in evolving silicic magma chambers. Geology, 31, 367–370.

Bindeman, I.N. and Valley, J.W. (2002) Oxygen isotope study of the Long Valley-Glass Mountain magmatic system, California: Isotope thermometry, and convection in large silicic magma bodies. Contributions to Mineralogy and Petrology, 144, 185–205.

Bodnar, R.J., Binns, P.R., and Hall, D.L. (1989) Synthetic fluid inclusions-VI. Quantitative evaluation of the decrepitation behaviour of fluid inclusions in quartz at one atmosphere pressure. Journal of Metamorphic Geology, 7, 229–242.

Brown, W.K. and Wohletz, K. (1995) derivation of the Weibull distribution based on physical principles and its connection to the Rossin-Rammler and lognormal distribution. Journal of Applied Physics, 78, 2758–2763.

Cabane, H., Laporte, D., and Provost, A. (2001) Experimental investigation of the kinetics of Ostwald ripening of quartz in silicic melts. Contributions to Mineralogy and Petrology, 142, 361–373.

——— (2005) An experimental study of Ostwald ripening of olivine and plagioclase in silicate melts: Implications for the growth and size of crystals in magmas. Contributions to Mineralogy and Petrology, DOI: 10.1007/500490-005-0002-2.

Cashman, S. and Cashman, K. (2000) Cataclasis and deformation-band formation in unconsolidated marine terrace sand, Humboldt County, California. Geology, 28, 111–114.

Castro, J.M., Cashman, K.V., and Manga, M. (2003) a technique for measuring 3D crystal-size distributions of prismatic microlites in obsidian. American Mineralogist, 88, 1230–1240.

Cavosie, A.J., Wilde, S.A., Liu, D.Y., Weiblen, P.W., and Valley, J.W. (2004) Internal zoning and U-Th-Pb chemistry of Jack Hills detrital zircons: a mineral record of early Archean to Mesoproterozoic (4348–1576 Ma) magmatism. Precambrian Research, 135, 251–279.

Crow, E.L. and Shimizu, K., 1988, Lognormal distributions: Theory and applications. 387 p. Dekker, New York.

Dacey, M.F. and Krumbein, W.C. (1979) Models of breakage and selection for particle size distributions. Mathematical Geology, 11, 193–222.

Diemer, R.B. and Olson, J.H. (2002) A moment methodology for coagulation and breakage problems: Part 1 - analytical solution of the steady-state population balance. Chemical Engineering Science, 57, 2193–2209.

Eberl, D.D., Drits, V.A., and Srodoñ, J. (1998) Deducing growth mechanisms for minerals from the shapes of crystal size distributions. American Journal of Science, 298, 499–533.

——— (2001) User's guide to GALOPER—a program for simulating the shapes of crystal size distributions—and associated programs. U.S. Geological Survey Open-File Report OF00-505, 44 p.

Eberl, D.D., Kile, D.E., and Drits, V.A. (2002) On geological interpretations of crystal size distributions: Constant vs. proportionate growth. American Mineralogist, 87, 1235–1241.

Engelder, J.T. (1974) Cataclasis and the generation of fault gauge. Geological Society of America Bulletin, 85, 1515–1522.
Englman, R. (1991) Fragments of matter from a maximum-entropy viewpoint. Journal of Physics-Condensed Matter, 3, 1019–1053.
Epstein, B. (1947) The mathematical description of certain breakage mechanisms leading to the logarithmico-normal distribution. Journal of the Franklin Institute, 244, 471–477.
Ferkinghoff-Borg, J., Mogens, H., Jensen, M.H., Mathiesen, J., Olesen, P., and Sneppenk, K. (2003) Competition between diffusion and fragmentation: An important evolutionary process of nature. Physical Reviews Letters, 91, art no. DOI: 10.1103/PhysRevLett.91.266103
Gualda, G.A.R., Cook, D.L., Chopra, R., Qin, L., Anderson, A.T. Jr., and Rivers, M. (2004) Fragmentation, nucleation and migration of crystals and bubbles in the Bishop Tuff Rhyolitic Magma. Transactions of the Royal Society of Edinburgh: Earth Sciences (Special volume, 5th Hutton Symposium on the Origin of Granites and Related Rocks), 95, 375–390.
Higgins, M.D. (1998) Origin of anorthosite by textural coarsening: quantitative measurements of a natural sequence of textural development. Journal of Petrology, 39, 1307–1323.
Higgins, M.D. (1994). Numerical modeling of crystal shapes in thin sections: Estimation of crystal habit and true size. American Mineralogist, 79, 113–119.
Ishii, T. and Matsushita, M. (1992) Fragmentation of long thin glass rods. Journal of the Physical Society of Japan, 61, 3474–3477.
Jerram, D.A. and Cheadle, M.J. (2000) On the cluster analysis of rocks. American Mineralogist, 85, 47–67.
Jerram, D.A., Cheadle, M.J., and Philpotts, A.R. (2003) Quantifying the building blocks of igneous rocks: Are clustered crystal frameworks the foundation? Journal of Petrology, 44, 2033–2051.
Kile, D.E. and Eberl, D.D. (2003) On the origin of size-dependent and size-independent crystal growth: Influence of advection and diffusion. American Mineralogist, 88, 1514–1521.
Kapteyn, J.C. and van Uven, M.J. (1903) Skew frequency curves in biology and statistics. Groningen. Astronomical Laboratory, Noordhoft.
Ketcham, R.A. and Carlson, W.D. (2001) Acquisition, optimization and interpretation of X-ray computed tomographic imagery: applications to the geosciences. Computers in Geosciences-UK, 27, 381–400.
Kolmogorov, A.N. (1941) On the lognormal distribution law of the dimensions of particles under pulverization. Doklady of the Akademy of Sciences of the USSR, 31, 99–101.
Line, W.R. and Aradine, P.W. (1937) Determination of quartz in the presence of other silicates. Industrial Engineering Chemical Analysis Edition, 9, 60–63.
Lipman, P., Dungan, M., and Bachmann, O. (1997) Comagmatic granophyric granite in the Fish Canyon Tuff, Colorado: Implications for magma-chamber processes during a large ash-flow eruption. Geology, 25, 915–918.
Luhr, J.F. and Melson, W.G. (1996) Mineral and glass compositions in June 15, 1991, pumices: evidence for dynamic disequilibrium in the dacite of Mt. Pinatubo. In C.G. Newhall R.S. Punongbayan, Eds., Fire and Mud: Eruptions and Lahars of Mt. Pinatubo, Philippines, p. 733–750. University Washington Press, Seattle, Washington.
Madras, G. and McCoy, B.J. (2002) Dynamics of crystal size distributions with size-dependent rates. Journal of Crystal Growth, 243, 204–213.
Mahmood, K. (1973) Lognormal size distribution of particulate matter. Journal of Sedimentary Petrology, 43, 1161–1166.
Mandelbrot, B.B. (1983) The fractal geometry of Nature. Freeman, New York.
Marchisio, D.L., Vigil, R.D., and Fox, R.O. (2003) Quadrature method of moments for aggregation-breakage processes. Journal of Colloid and Interface Science, 258, 322–334.
Marsh, B.D. (1998) On the interpretation of crystal size distributions in magmatic systems. Journal of Petrology, 39, 553–599.
McCoy, B.J. (2001) A new population balance model for crystal size distributions: Reversible, size-dependent growth and dissolution. Journal of Colloid and Interface Science, 240, 139–149.
Meibom, A. and Balslev, I. (1996) Composite power laws in shock fragmentation. Physical Reviews Letters, 76, 2492–2495.
Middleton, G.V. (1970) Generation of the lognormal frequency distribution in sediments. In M.A. Romanova and O.V. Sarmanov, Eds., Topics in mathematical geology, p. 34–42. Consultatants bureau, New York.
Nelson, V.E. and Rubin, A.E. (2002) Size-frequency distributions of chondrules and chondrule fragments in chondrites; implications for parent-body fragmentation of chondrules. Meteoritics and Planetary Science, 37, 1361–1376.
Oddershede, L., Dimon, P., and Bohr, J. (1993) Self-organized criticality in fragmenting. Physical Reviews Letters, 71, 3107–3110.
Pallister, J.S., Hoblitt, R.P., Meeker, G.P., Knight, R.J., and Siems, D.F. (1996) Magma mixing at Mt Pinatubo: petrographic and chemical evidence from 1991 deposits. In C.G. Newhall R.S. Punongbayan, Eds., Fire and Mud: Eruptions and Lahars of Mt. Pinatubo, Philippines, p. 687–732. University Washington Press, Seattle, Washington.
Peppard, B.T., Steele, I.M., Davis, A.M., Wallace, P.J., and Anderson, A.T. (2001) Zoned quartz phenocrysts from the rhyolitic Bishop Tuff. American Mineralogist, 86, 1034–1052.
Poldervaart, A. (1956) Zircon in rocks 2: Igneous rocks. American Journal of Science, 254, 521–554.
Randolph, A.D. and Larson, M.A. (1988) Theory of Particulate Processes, 2nd ed. 369 p. Academic Press, New York.
Rudashevsky, N.S., Burakov, B.E., Lupal, S.D., Thalhammer, A.R., and Saini-Eidukat, B. (1995) Liberation of accessory minerals from various rock types by electric-pulse disintegration-method and application. Transactions of the Institution of Mining and Metallurgy, 104, C25–C29.
Saini-Eidukat, B. and Weiblen, P.W. (1996) Liberation of fossils using high voltage electric pulses. Curator, 39, 139–144.
Sammis, C.G. and Biegel, R.L. (1989) Fractals, fault-gouge, and friction. Pure and Applied Geophysics, 131, 255–271.
Sammis, C.G., Osbourne, R.H., Anderson, J.L., Banerdt, M., and White, P. (1986) Self-similar cataclasis in the formation of fault gouge. Paleoph, 124, 57–78.
Schwindinger, K. (1999) Particle dynamics and aggregation of crystals in a magma chamber with application to Kilauea Iki olivines. Journal of Volcanology and Geothermal Research 88, 209–38.
Shimizu, K. and Crow, E.L. (1988) History, genesis, and properties of lognormal distributions. In: Crow, E.L. and Shimizu, K. (Eds) Lognormal distributions: Theory and applications. New York, Dekker, pp. 1–25.
Sotolongo-Costa, O., MorenoVega, Y., LloverasGonzalez, J.J., and Antoranz, J.C. (1996) Criticality in droplet fragmentation. Physical Reviews Letters, 76, 42–45.
Sotolongo-Costa, O., Rodriguez, A.H., and Rodgers, G.J. (2000) Dimensional crossover in fragmentation. Physica A, 286, 638–642.
Spicer, P.T. and Pratsinis, S.E. (1996) Coagulation and fragmentation: Universal steady-state particle-size distribution. AICHE Journal, 42, 1612–1620.
Tavassoli, Z. and Shirvani, A.E. (2000) Models of fragmentation with power-law log-normal distribution. Physica A, 286, 29–44.
Tait, S. (1992) Selective preservation of melt inclusions in igneous phenocrysts. American Mineralogist, 77, 146–155.
Tait, S., Thomas, R., Gardner, J., and Jaupart, C. (1998) Constraints on cooling rates and permeabilities of pumice in an explosive eruption jet from colour and magnetic mineralogy. Journal of Volcanology and Geothermal Research, 86, 79–91.
Turcotte, D.L. (1997) Fractals and chaos in geology and geophysics, 2nd Edition. 398 p. Cambridge University Press, U.K.
——— (2002) Fractals in petrology. Lithos, 65, 263–271.
Vance, J.A. (1969) On synneusis. Contributions to Mineralogy and Petrology, 24, 7–29.
Wallace, G. and Bergantz, G. (2002) Wavelet-based correlation (WBC) of zoned crystal populations and magma mixing. Earth and Planetary Science Letters, 202, 133–145.
Wallace, P., Anderson, A.T., and Davis, A.M. (1999) Gradients in H_2O, CO_2, and exsolved gas in a large volume silicic magma system; interpreting the record preserved in melt inclusions from Bishop Tuff. Journal of Geophysical Research, B104, 20097–20122.
Wanamaker, B.J., Wong T.-F., and Evans, B. (1990) Decrepitation and crack healing of fluid inclusions in San Carlos Olivine. Journal of Geophysical Research, 95, 15,623–15,641.
Wohletz, K.H., Sheridan, M.F., and Brown, W.K. (1989) Particle-size distributions and the sequential fragmentation transport-theory applied to volcanic ash. Journal of Geophysical Research, 94, 15703–15721.
Zhang, Y. (1998) Mechanical and phase equilibria in inclusion-host systems. Earth and Planetary Science Letters, 157, 209–222.

MANUSCRIPT RECEIVED MARCH 14, 2004
MANUSCRIPT ACCEPTED MAY 5, 2005
MANUSCRIPT HANDLED BY RICHARD KETCHAM

APPENDIX 1: STATISTICS OF PARTICLE SIZE-FREQUENCY DISTRIBUTIONS

Different kinds of fragmentation processes result in several types of size (mass) –frequency distribution, which are described below.

Lognormal distribution. A two-parameter lognormal distribution $\Lambda = (\alpha, \beta^2)$ is defined by the frequency curve of a parameter x (e.g., size, surface area, or volume), and is given as:

$$f(x) = \frac{1}{x\beta\sqrt{2\pi}} \exp\left\{-\frac{\left[\ln(x)-\alpha\right]^2}{2\beta^2}\right\} \quad \text{(A1)}$$

where α and β are the mean and the standard deviation respectively. The three-parameter distribution, $\Lambda = (\alpha - \tau, \beta^2)$ (Shimizu and Crow 1988; Atchison and Brown 1957) includes an additional threshold parameter τ, in the $\ln(x-\tau)$ expression in [A1], making the frequency curve start with the value τ at $f(x) = 0$. For example, the three-parameter distribution may characterize crystal sizes with no crystals smaller than a threshold size (e.g., no microlites due to the retention in nucleation).

The great practical and theoretical value of lognormal distribution is that it is *dimension-invariant*, meaning that if volumes (or mass) are lognormally distributed, then linear size, or areas are also lognormally distributed. This comes as a general property of logarithms that if a variate X is lognormally distributed, its 1/3 power is also lognormally distributed: $\Lambda_{-3} = \Lambda(\alpha - 3\beta^2, \beta^2)$ (e.g., Aitchison and Brown 1957, p. 101). This property is important for stereological corrections. The loggamma probability law, which is discussed in the text, has the same property.

Fractal, or power-law, distribution. A two-parameter ("true") fractal distribution is defined (e.g., Mandelbrot 1983; Turcotte 1997) as:

$$f(x) = \frac{C}{x^D} \tag{A2}$$

with C as a constant, and the power D called the fractal dimension. The multifractal distribution may contain an additional parameter(s) β in the power D (e.g., Turcotte 2002).

Upon fragmentation of a crystal population with a number of particles per breakage cycle, called here the branching ratio, B, and the probability of breakage, F, the fractal dimension D can be determined from a simple relationship (Turcotte 1997):

$$D = 3\ln(B*F)/\ln B$$

The fractal distribution in the form (A2) is popular because it is *scale-invariant*, meaning that a petrographer will determine the same fragment (particle) size distribution regardless of magnification (e.g., quartz sand grain sizes in fault gouges, Sammis and Biegel 1989), or olivine in mantle nodules (Armienti and Tarquini 2002). Graphically fractal distribution is identified on a log-log scale of frequency vs. size:

$$\log f(x) = C - D\log x$$

that has a slope of D, the fractal dimension.

Weibull distribution. Weibull distribution is defined as (Brown and Wohletz 1995):

$$f(x) = \frac{N_T}{x_1}\left(\frac{x}{x_1}\right)^{\gamma} \exp\left\{-\frac{\left[x/x_1\right]^{\gamma+1}}{\gamma+1}\right\} \tag{A3}$$

where N_T is the total number of fragments in the distribution, and γ ($-1<\gamma<0$) is the shape parameter (analogous to the fractal dimension D). The Weibull distribution was proposed to best describe the sequential comminution process. Mathematically and graphically, the Weibull distribution looks intermediate between lognormal 1 and fractal 2 (see Fig. 1), but it does not have the intrinsic advantage of being dimension- or scale-invariant.

Loggamma distribution. The loggamma (factorial) distribution is defined as (e.g., Dacey and Krumbein 1979):

$$f(x) = [(n-1)!]^{-1}[-\ln(x)^{n-1}] \tag{A4}$$

Where n is a scale parameter defined by the number of breakage cycles, here defined for sizes $0 < x < 1$, when α, the shape parameter is 1. On a log-log diagram (Fig. 1), the loggamma distribution is concave down and its curvature decreases as n increases. It is, nonetheless, is significantly different from the fractal distribution. A mixed loggamma distribution can be visualized by graphical additions of loggamma distributions of different n. A mixed loggamma-lognormal distribution is intermediate between the two.